RSC Advances

ROYAL SOCIETY OF CHEMISTRY

www.rsc.org/advances

Theoretical and experimental study of folic acid conjugated silver nanoparticles through electrostatic interaction for enhance antibacterial activity

Angshuman Ray Chowdhuri[1], Satyajit Tripathy[2], Chanchal Haldar[1], Soumen Chandra[1], Balaram Das[2], Somenath Roy[2], Sumanta kumar Sahu[*1]

1 Department of Applied Chemistry, Indian School of Mines, Dhanbad 826004, Jharkhand, India

2 Immunology and Microbiology Laboratory, Department of Human Physiology with Community Health, Vidyasagar University, Midnapore-721102, India

* Corresponding author. E-mail: sahu.s.ac@ismdhanbad.ac.in, sumantchem@gmail.com

Fax: +91-326-2307772; Telephone: +91-326-2235936

Abstract

In this paper, folic acid conjugated silver nanoparticles (Ag NPs) is developed for enhance the antibacterial activity. Here triethylamine is used as a capping agent as well as reducing agent during the synthesis of silver nanoparticles. Folic acid is conjugated on the surface of functionalized silver nanoparticles through electrostatic interaction. The folic acid conjugated silver nanoparticles are characterized in terms of size and morphology by transmission electron microscopy (TEM) and field emission scanning electron microscopy (FESEM) respectively. The phase formation and surface functional groups of nanoparticles are analyzed by X-ray diffraction (XRD) and Fourier transform infrared (FTIR) respectively. Minimum inhibitory concentration study, minimum bactericidal concentration, growth pattern analysis and fluorescence carbon dot tagged nanoparticles uptake study reveal that folic acid conjugated silver nanoparticles show more prospective against both Gram-negative (*Escherichia coli*) and Gram-positive (*Staphylococcus aureus*) bacteria.

Keywords: Silver nanoparticles; Folic acid; Carbon Dots; Antibacterial activity; Computational study**.**

1. Introduction

In recent years, there has been a phenomenal impetus for the development of novel, multifunctional materials for medicine [1-3]. Among them Antibacterial materials play significant roles in treating infectious diseases caused by pathogenic bacteria [4-6]. Nanoscale materials have emerged as novel antimicrobial agents. Some of these agents were found to be cytotoxic against bacteria but not against mammalian cells making, antibacterial drugs. The use of inorganic nanoparticles has attracted a lot of interest because of their reliable antimicrobial activities found to be effective at low concentrations [7].

Drawbacks for conventional antimicrobial agents are not only the development of multiple drug resistance, but also adverse side effects. Drug resistance enforces high dose administration of antibiotics, often generating intolerable toxicity. This has prompted the development of alternative strategies to treat bacterial diseases [8]. Especially, several classes of nanoparticles have proven their effectiveness for treating infectious diseases [9]. Therefore, currently the rapid use of nanotechnology for medical applications opens up a new prospect in antibacterial research. Till now number of nanomaterials are reported as antibacterial agents [10]. Among them silver nanoparticles have sparked significant interest. The effectiveness of silver nanoparticles as an antibacterial agent has been known for a long time [11-13]. To improve further antibacterial effects, we have introduced here folic acid conjugated silver nanoparticles.

Folic acid has been extensively used as a targeting ligand towards cancer cells due to its high binding affinity for the folate receptors [14, 15]. Folic acid is conjugated with nanoparticles through the chemical bond by multistep synthetic route. Roger et al. synthesized folic acid functionalized poly (D, L-lactide-co-glycolide) nanoparticles loaded with paclitaxel to enhance the oral absorption of drugs with poor oral bioavailability [16]. Lin et al. designed Folic acid conjugated Pluronic F127 magnetic nanoparticle clusters for combined targeting, diagnosis, and therapy applications [17]. We have also synthesized folic acid functionalized different nanoparticles for potential tumour targeting [18, 19]. But in this work folic acid is conjugated with silver nanoparticles without any chemical bond for enhancement of the antibacterial activity.

It is possible that folic acid functionalized silver nanoparticles enhance the interactions with the cell membrane of the bacterial cell. In this context, the presence of folic acid on Ag nanoparticles plays a crucial role, as this ligand may essential nutrient for nucleotide synthesis of the bacteria, helps to transport the nanoparticle through endocytosis across the plasma membrane into the cytoplasm [20, 21]. This explanation is also consistent with the findings of our previously published report in which vancomycin loaded folic acid functionalized chitosan nanoparticles were used for anti VRSA agent [22]. Till now a number of investigations have dealt with the design, fabrication and antibacterial property of silver nanoparticles but the fundamental point is the conjugation of folic acid influences the antibacterial effect of nanoparticles still remains unaddressed.

In this study, a convenient physical interaction has been developed to enhance the antibacterial property. Here an environmentally friendly and one step method is developed for the preparation of Ag nanoparticles using triethylamine as a reducing agent as well as capping agent. Then folic acid has been attached with triethylamine functionalized silver nanoparticles by physical interaction to increase the bacterial toxicity. To prove the increment of attachment of nanoparticles with the bacterial cell, a highly florescent carbon dot is attached with the synthesized nanoparticles by electrostatic attraction.

2. Experimental Method

2.1. Material

Silver Nitrate ($AgNO_3$) was obtained from RANKEM, Triethylamine (TEA), dimethyl sulfoxide (DMSO), Ethanol and dichloromethane was purchased from MERCK, Folic Acid (FA) and EDC-HCL was taken from SPECTROCHEM, Orange Juice from local market. All chemicals were used without further purification. Nutrient broth and Luria broth were purchased from Himedia, India. Alcohol and other chemicals were procured from Merck Ltd., SRL Pvt. Ltd. Mumbai India.

2.2. Synthesis of Silver Nanoparticle (Ag@TEA)

Silver nanoparticles were synthesised by previously reported method with slight modification [23]. Briefly, 0.16 g of $AgNO_3$ was dissolved in 10 ml of Millipore water in a

RB flask to prepare a 1 M solution. To this solution, 1.37 ml TEA was added drop wise in an argon atmosphere at 45 °C temperature. Colour of the solution turns black after addition of TEA indicates nanoparticles were formed and stirring was continued for 360 min. The nanoparticles were washed several times with ethanol, followed by centrifugation (5000 rpm, 10 min), to remove unbounded TEA. The nanoparticles were then dried at 40 °C temperature under vacuum for 24 h.

2.3. Preparation of Folic acid functionalised Silver Nanoparticle (Ag@TEA@FA)

To prepare folic acid conjugated Silver nanoparticle, 176.5 mg of folic acid and 76.6 mg EDC were dissolved in 40 ml DMSO-water medium (1:1) at room temperature by 3 h. Then 130 mg Ag nanoparticles were added to that mixture solution with continuous stirring at room temperature for 12 h. The nanoparticles were collected by centrifugation at 5000 rpm. The product was dried in vacuum at room temperature. The functionalised material was yellowish in colour.

2.4. Synthesis of Carbon Dots (CDs) attached Ag@TEA and Ag@TEA@FA

Firstly, Carbon Dots were synthesized by previously reported method with slight modification [24]. Briefly, 20 ml of orange juice (absolutely pulp-free) was mixed with 15 ml ethanol, and then the mixture was transferred into a 50 ml Teflon-lined stainless-steel autoclave and heated at 125 °C for 150 min (1 °C/min). After the reaction is over, the autoclave was cooled down naturally. The resulted dark brown solution was washed with dichloromethane to remove the unreached organic moieties. The aqueous solution was centrifuged at 4000 rpm for 10 min to separate the less-fluorescent deposit. After that in carbon dots solution, EDC-HCL was added to enrich the reactivity of surface COOH group of carbon dots. Then, Ag@TEA and Ag@TEA@FA were added separately to the above carbon dots solution and stirred the reaction for 12 h. The carbon dot attached silver Ag@TEA and Ag@TEA@FA was collected by centrifugation at 5000 rpm.

2.5. Instrumentation

Attachment of surface functional groups was investigated by FTIR spectroscopy (Thermo Nicolet Nexux FTIR (model 870) and TGA. TGA measurement was performed by TGA 2850 thermogravimetric analyzer (TA instruments) under N_2 atmosphere. The phase formation and

crystallographic state of Silver nanoparticles were determined by XRD with an Expert Pro (Phillips) X-ray diffractometer using Cu Kα. The particle size and microstructure were studied by high-resolution transmission electron microscopy in a JEOL 3010, Japan operating at 200 keV. FESEM analysis was performed by Supra 55 with Air Lock chamber for scientific research. Growth curves of bacterial cell cultures were attained through repeated measures of the optical density (O.D.) at 600 nm by UV-VIS spectroscopy were taken at 25 °C with a Perkin-Elmer Lambda-20 spectrometer. The fluorescence intensity of each sample was analyzed under fluorescent microscope for detection of fluorescence intensity in bacterial cells.

2.6. Computational study

All type of interactions between triethylamine functionalized silver nanoparticle with folic acid and full geometry optimization of triethylamine and folic acid were performed with Gaussian 03 [25] program package. For visualization we have used GaussView 5.0 [26]. To reduce the computational load while maintain the real picture of interactions as much practical as possible we used hartree-fock (HF) method. All the Hartree-Fock (HF) calculations are done for isolated molecules in gaseous phase without any symmetry constrain. Ground state geometry of folic acid optimized by using HF/6-311g (d,p) level of theory. HF/LANL2MB basis set with an effective core potential for Ag was used in its restricted and unrestricted form, and a few combination of basis set were tested for getting the best computational model which produce the best geometric structure. For sake of simplicity we have considered one silver atom as a model for silver nanoparticle. We have performed vibrational frequency calculations at the same level of theory, lack of imaginary frequencies ensures that the optimized geometry represents the local minima and that there are only positive Eigen value.

2.7. Preparation of bacterial suspension

The bacterial strain of Gram-positive bacteria (*Staphylococcus aureus*) and Gram-negative bacteria (*Escheria coli*) were grown at 37 °C overnight in nutrient agar broth. The bacterial culture was centrifuged at 15000 rpm for 15 minutes. The pallets were suspended and washed with sterile phosphate buffer saline (PBS). The bacterial suspension was adjusted by serial dilution in PBS to final concentration of approximately 5×10^6 in 100 µl by using a

UV-spectrophotometer (Schimadzu, USA) at an absorbance of 620 nm, the viable bacterial count was adjusted to approximately 1.0×10^9 colony forming units (CFU)/ml.

2.8. Determination of minimum inhibitory concentration (MIC)

The minimum inhibitory concentration (MIC), concentration of the Ag@TEA and folic acid conjugated silver nanoparticle (Ag@TEA@FA) where no visible growth appeared in the broth tube, were determined against Gram-positive bacteria (*S. aureus)* and Gram-negative bacteria *(E. coli)* by a slight modification of the described method of Wang et al [27].

2.9. Determination of minimum bactericidal concentration (MBC)

The minimum bactericidal concentration (MBC) of the Ag@TEA and Ag@TEA@FA were evaluated against *S. aureus* and *E. coli* by slight modification of the method described by Ericsson and Sherris [28]. After the MIC test, bacteria from each test tube were checked overnight at 37 °C. The MBC value was that concentration of the nanoparticles where no visible growth appeared on the agar plate.

2.10. Disc Agar Diffusion (DAD) method

The disc diffusion method [29] was used to evaluate the antimicrobial activity of Ag@TEA and Ag@TEA@FA at MIC concentration respectively against Gram-positive (*Staphylococcus aureus*) and Gram-negative bacteria (*Escheria coli*). This method was performed in Luria Bertani (LB) medium solid agar Petri dish. Briefly, 6 mm sterile paper discs were impregnated with nanoparticles and placed on *Staphylococcus aureus* and *E. coli* cultured agar plate. Agar plate was then incubated for 24 h at 37 °C and inhibition zone was monitored. After incubation the presence of bacterial growth inhibition around the samples were absorbed.

2.11. Determining the growth curves of bacterial cells exposed to MIC concentrations of nanoparticles

To examine the growth patterns, the Gram-positive bacterial cells were charged by Ag@TEA and Ag@TEA@FA nanoparticles at MIC concentrations (100 and 10 μg/ml) respectively, and the Gram-negative bacterial cells also treated by Ag@TEA and

Ag@TEA@FA, at MIC concentrations, (250 μg/ml and 10 μg/ml) respectively after adjustment of bacterial concentration to 10^6 CFU/ml. Each culture was incubated in a shaking incubator at 37 °C and optical density at 600 nm was measured at different time interval [30].

2.12. Nanoparticle uptake efficacy

To examine the nanoparticles incorporation into the bacterial cells, carbon dots (CDs) were attached with Ag@TEA and Ag@TEA@FA nanoparticles in MIC concentrations. The bacterial concentration was adjusted to 10^6 CFU/ml. Each culture was incubated in a shaking incubator at 37 °C for overnight. The cells were washed twice with phosphate buffered saline to remove any unutilized CDs attached nanoparticles. The fluorescence intensity of each sample was analyzed under fluorescent microscope for detection of fluorescence intensity in bacterial cells.

2.13. Data analysis

The statistical analysis was performed by using a statistical package, Origin 6.1, Northampton, MA 01060, USA) with student's *t* tests, $p < 0.05$ as a limit of significance.

3. Result and Discussion

In the last decade increasing interest has been devoted to the design of silver nanoparticles for their potential antimicrobial activities. Nevertheless, various studies have also reported that functionalised Ag NPs may induce significant cytotoxicity both *in vitro* and *in vivo* [31]. The mechanism of Ag NPs induced cytotoxicity is not completely understood. Many recent investigations have attributed the toxicity to the generation of ROS or oxidative stress or Ag^+ ion release from the nanosized material [32-34].

3.1. XRD Analysis

Powder XRD analysis exhibits the characteristics of the crystallographic structure and physical properties of the materials, shown in Figure 1(a). The Ag @ TEA and Ag @ TEA @ FA NPs show identical characteristic diffraction peaks at 2 Theta = 38.14°, 44.30°, 64.53°, 77.36° which corresponds to the reflection plane indices of (1 1 1), (2 0 0), (2 2 0), (3 1 1), respectively. All detected diffraction peaks could be attributed to the characteristic peaks of Silver nanoparticles (JCPDS card no. 04-0783). The mean crystallite size was found to be

around 14 nm. This reveals that the surface modification and conjugation of the Ag nanoparticle by folic acid do not lead to their phase change.

3.2. FTIR Analysis

The conjugation of Silver nanoparticles with folic acid is characterized by FTIR analysis. FTIR spectrum of the Ag nanoparticles synthesized using triethylamine and folic acid conjugation of the same was shown in Figure 1(b). The Ag@TEA@FA was characterized to obtain detailed information about conjugation of Folic acid for the peaks at 3000, 2337, 2367, 1600, 1510, 1408, 1350, 1030 cm^{-1}. The characteristic band at 1494 cm^{-1} corresponds to the phenyl ring of folic acid and the other bands are also identified in the spectrum confirms the successful conjugation of folic acid on the Ag NPs. Peak at 1600 cm^{-1} was attributed to amide C-O stretching and the broad peak near 3394 cm^{-1} was designated as an O-H stretching vibration.

3.3. Surface Morphology Analysis

To investigate the morphology of Ag@TEA@FA nanoparticles, TEM image was taken. From the TEM image of Figure 2 (a) shows a spherical morphology having a uniform size. To prevent the large agglomeration due to vanderwaal's or Coulomb's force, here TEA acts as a stabiliser. Field emission scanning electron microscopy (FESEM) analysis demonstrated that, with using TEA, the surface of the nanoparticles were composed of uniform, closely packed and well-aligned particles as shown in Figure 2 (b). From TEM analysis, the average diameter of the particles was calculated to be 10 ± 5 nm with significantly narrow size distribution [Figure 2 (c)]. We can control the nanoparticle size by increasing the molar ratio of TEA.

The energy dispersive X-ray spectroscopy (EDX) of the spherical Ag@TEA nanoparticles is shown in Figure 2(d). The EDX quantitative analysis confirmed that the nanostructure contained about 91.51 wt. % Ag with 4.5 wt. % and 2.5 wt. % Carbon and Nitrogen respectively. Throughout the scanning range of binding energies, no obvious peak belonging to impurity is detected. The result indicates that the product is composed of high purity Ag nanoparticles.

3.4. Interaction of Surface modified silver nanoparticle with the folic acid

3.4.1. Geometry optimization

Gas phase optimization of folic acid was performed with HF/6-311g (d, p) and HF/LANL2MB level of theory as shown in Figure 3. Calculation reveals that optimized structure contains H-bond between 10O and 50H with a bond distance 1.783Å. Zero imaginary frequency ensures the minimum energy state for the molecule. To investigate the reactive sites of the structure the molecular electrostatic potential were evaluated using the HF/6-311g (d,p) method. Molecular electrostatic potential is the most useful electrostatic property to study the relation between the structure and reactivity. Electrostatic potential created by the nuclei and electrons of a molecule in the surrounding space is well established as a guide to the interpretation and prediction of molecular behaviour. It is a very useful tool in studying both elecrophilic and nucleophilic process [35-39]. In particular it is well suited for studies that involve the identification of key features necessary for the recognition of one molecule by another.

To predict the reactive sites of electophilic and nucleophilic attack for the investigated molecule, the Molecular Electrostatic Potential (MEP) at the HF/6-311g (d,p) optimized geometry was calculated and shown in Figure 4(a). As seen from the Figure 4(b) negative electron density is basically populated over the oxygen and nitrogen atoms. And consequently the net positive charges spread over the few hydrogen atoms namely 38H, 43H, 46H, 47H, 48H and 51H. The middle point of the molecules is approximately neutral but the presence of 17N in the bottom of the valley makes molecule somewhat more electron rich. The nucleophilic site is represented by red color and electrophilic site is represented by blue colour. On the other hand in triethylamine the negative charge concentrate mainly on the central nitrogen atom can be regarded as potential electrophilic site shown in Figure 4(b). From the molecular electrostatic potential of TEA it has been seen that for effective interaction we have to place the silver atom on top of the negatively charge surface of nitrogen atom. For the optimization again we were used HF/LANL2MB level of theory with an effective core potential for silver atom. Frequency calculations were carried out using the optimized geometry and it was verified that the structures represent true minima of the potential energy surface. MEP of Ag@TEA Cluster clearly showed that there was no Ag-TEA covalent bond found in the Optimized geometry, only an electrostatic interaction exists in the Ag-TEA cluster shown in Figure 4. The di-TEA@Ag cluster was also optimized and optimized geometry corresponded to minima on the potential energy surface was verified by the frequency analysis with the same level of theory. Where di-TEA@Ag cluster was design by placing one silver atom in between two triethylamine molecules.

The interaction between Ag (I) and TEA found direct chemical bond between the Ag (I) and TEA. Complete optimization of Ag+-TEA cluster was done with the help of RHF/LANL2MB level of theory.

3.4.2. Computational method

In search of the nature of interactions of surface modified silver nanoparticle with the folic acid, interactions were modelled by placing the surface modified silver nanoparticle in the different electrophilic position of folic acid. The equilibrium geometrics of the cluster formed between surface modified silver nanoparticle and folic acid were obtained by using HF/LANL2MB level of theory. By examine the various sites four TEA@Ag@FA cluster and three di-TEA@Ag@FA cluster were obtained. Frequency calculations were performed to verify that the structure represented the true minima of the potential energy surface. Change in energy i.e. the force of attraction between the TEA modified silver nanoparticles and folic acid was calculated using the equation:

$\Delta E_{interaction}$ (Ag@TEA@FA) = E (Ag@TEA@FA) - E (FA) - E (Ag@TEA)

Where $\Delta E_{interaction}$ (Ag@TEA@FA) = formation energy change of Ag@TEA@FA cluster, E (FA) = energy of folic acid, and E (Ag@TEA) = energy of TEA modified silver nanoparticles i.e. energy of TEA…Ag cluster.

We selected four different conformations for the present study by placing the TEA modified silver nanoparticles in close vicinity of four most electrophilic site of the folic acid and three different conformation by placing di-TEA@Ag in the various electrophilic sites of the folic acid. All initial clusters were fully geometry optimized. For TEA@Ag@FA cluster the optimized geometries are designated by (a) Molecular cluster 1, (b) Molecular cluster 2, (c) Molecular cluster 3 and (d) Molecular cluster 4 and di-TEA@Ag@FA optimized geometries are designated by (e) Di-Molecular Cluster 1 (f) Di-Molecular Cluster 2 and (g) Di-Molecular Cluster 3 shown in Figure 5.

It is observed from the calculation that the out of four TEA@Ag@FA cluster molecular cluster 1 shows the most weak interaction position, remaining three complexes show a very strong electrostatic interaction with the TEA@Ag nanoparticle. While all the di-TEA@Ag@FA clusters show less interaction energy in comparison to the TEA@Ag@FA cluster. Change in cluster formation energy suggests an appreciable amount of charge transfer

from electron rich centre to the empty d orbital of silver atom and hence a stronger interaction between TEA@Ag and Folic acid.

3.4.3. Nature of interaction

In terms of bond distance, it is observed that the Ag…N or Ag…O interaction distance is comparable with the interaction distance, found in the literature. Also it is evident from the calculation that the Ag-N and Ag-O bond distances are much higher in comparison to the covalent bond distances of Ag-N and Ag-O, found in the crystal structure reported in the literature.

It is clear from the table S1 that significantly high atom distances between the Ag, TEA and folic acid do not support the existence of covalent bond between them but indicating the presence of weak interactions.

By examine the high interaction energies among the molecular clusters ranging from 10.87 to 71.99 Kcal/mol prove the presence of electrostatic interaction between the interacting atoms within the cluster. Electrostatic interaction exists between the Ag and the neighbour's atoms through the electron transfer from the donor to the acceptor atom and the transfer of electron density can be visualized by monitoring the natural charge density difference between the individual components and the molecular clusters.

Most importantly the natural charge density over silver atom before the cluster formation and after cluster formation are -0.20946 and -0.336 (cluster 1) respectively. The more negative values confirm a significant amount of electron transfer from neighbouring atoms to the silver atom. Other molecular clusters also show a significant natural charge transfer to the silver atom. The natural charge density over silver atom in molecular cluster 2 is -0.330, in molecular cluster 3 is -0.365 and in molecular cluster 4 is -0.378. Increases natural charge density over silver atom in the cluster 1, 3 and 4 makes more strong interaction with the neighbouring atoms which is also reflected from their increasing binding energy interaction. Binding interaction energies for molecular cluster 1, molecular cluster 2, molecular cluster 3 and molecular cluster 4 are 14.57, 65.54, 71.13 and 71.99 kcal/ mol respectively.

The Di-TEA@Ag@FA cluster shows weaker interaction in comparison to the mono-TEA cluster shown in table S2. This phenomenon can be easily explained by the available space requirement for the effective interaction. In the mono-TEA cluster the silver nanoparticle is covered from one side by the TEA, but in Di-TEA@Ag@FA silver nanoparticle is almost

entirely covered by TEA from every corner shown in Figure 4(d). That is why Ag nanoparticles barely get a chance to come closer to the nucleophlic site of folic acid. But still the interaction energies are sufficiently high for holding the folic acid strongly.

From the Natural Bond Orbital (NBO) analysis we can identify the two centered bonds between atoms in the natural Lewis structure. The Lewis structure is accepted if all orbital's of the formal Lewis structure exceed the occupancy threshold (default = 1.90 electrons). We have examined the NBO calculations data and we do not find any effective bond between silver atoms to that of any other atoms of the molecular cluster. Second order perturbation theory analysis of fock matrix indicates large number of non-bonding interactions within the each molecular cluster. The interactions between donors and acceptors result in a loss of occupancy from the localized NBO of the idealized Lewis structure of the donor into an empty Non-Lewis orbit of acceptor. Although the second order perturbation energies (often called as the stabilization energies or interaction energies) of most of the non-bonding interactions are considerably very low. A large number of such non-bonding interactions increase the stability of the molecular clusters.

Based on the above calculations and discussion it is very much clear to say that there is no such covalent bond exists between the interacting molecular species only charge transfer or conjugative interactions holds the TEA modified silver nanoparticle and folic acid.

3.5. Minimum Inhibitory Concentration

In this study we compared the efficacy of bactericidal activity of our synthesized Ag@TEA and Ag@TEA@FA nanoparticles against *S. aureus* and *E. coli*. The minimum inhibitory concentration (MIC) of Ag@TEA and Ag@TEA@FA against *S. aureus* and *E. coli* were evaluated. Figure S2 (A, C) [supporting information] is showing that the MIC of Ag@TEA against *S. aureus* and *E. coli* was 100 µg/ml and 250 µg/ml respectively. But when, Ag@TEA@FA was charged against the bacteria the MIC concentration decreased at 10µg/ml in both, shown in Figure S2 (B, D). Though the antibacterial activities of the Ag@TEA@FA against the Gram-positive *S. aureus* and Gram-negative *E. coli* were identical but more bactericidal against *E. coli* than only Ag@TEA.

3.6. Minimum Bactericidal Concentration

To be confirming about the bactericidal activity of Ag@TEA@FA we followed the MBC study. The particular particle concentration was noted for each strain where no visible growth appears on the agar plate, both in the case of Ag@TEA and Ag@TEA@FA. In the case of Ag@TEA, charged against the Gram-positive strain and Gram-negative strain, the MBC value was found at 500μg/ml in both (Figure not shown) whereas the MBC value was found at 25μg/ml in both strain against Ag@TEA@FA (Figure 6).

3.7. Disc Agar Diffusion (DAD) method

DAD study was followed for visual comparison between the Ag@TEA and Ag@TEA@FA. Figure 6 exhibits the inhibition zone of the two particles. The result showed that Ag@TEA@FA (i) is more effective than Ag@TEA (ii) against Gram-positive and Gram-negative both.

3.8. Growth curves of bacterial cells treated with different concentrations of Ag NPs

The growth pattern of bacterial cells after treatment with Ag@TEA and Ag@TEA@FA has been shown in Figure 7(C). The results revealed that the bacterial growths of cells treated with Ag@TEA and Ag@TEA@FA were inhibited but the better bactericidal activity found from the second. Interestingly, upon comparison of the bacterial growth curves, the growth curves of the Ag@TEA@FA treated bacteria indicated a faster growth inhibition of *E. coli* than of *S. aureus*.

3.9. Bacterial Morphology change after contact with Ag@TEA@FA nanoparticles :

The Ag@TEA@FA nanoparticles successfully inhibited the growth of *E. coli* and *S aureus*. We therefore examined the morphology changes of *E. coli* cells before and after treatment to the Ag@TEA@FA nanoparticles by using FESEM. The controlled *E. coli* cells have rod like shape and unbroken surfaces, shown in Figure 7(A). After acquaintance to 10μg/ml Ag@TEA@FA for 12 h, the morphology of bacteria was significantly deviated and cytoplasm of some bacteria has leaked out [Figure 7 (B)].

3.10. Nanoparticles uptake efficiency

Figure 8 shows that the fluorescence intensity in Ag@TEA@FA treated bacterial cells is more than Ag@TEA treated bacteria. As the nanoparticles were conjugated with CDs, the

result reveals that Ag@TEA@FA has been uptake more by bacteria than Ag@TEA. The result indicates that the both *S. aureus* and *E. coli* are more susceptible to synthesized Ag@TEA@FA but the Gram-positive bacteria are less susceptible to Ag@TEA@FA than Gram-negative bacteria. It may be due to the charge of peptidoglycan molecules in the bacterial cell wall. Gram-positive bacteria have more peptidoglycan than Gram-negative bacteria because of their thicker cell walls and as peptidoglycan is negatively charged and silver ions are positively charged, more silver may get trapped by peptidoglycan in Gram-positive bacteria than in Gram-negative bacteria [40].

4. Conclusion

In this paper, a novel technique has been developed to synthesize folic acid conjugated silver nanoparticles to enhance the antibacterial activity in comparison to pure silver nanoparticles. From the FTIR and TGA results, it is confirmed that the folic acid is conjugated with silver nanoparticles through electrostatic interaction. Moreover, theoretical simulations further elucidate the interactions of folic acid and silver nanoparticles are electrostatic in nature. Fluorescent carbon dots are successfully conjugated with silver nanoparticles for uptake study in bacteria. This folic acid conjugated silver nanoparticles have lowered the level of the MIC and MBC values and act as effective antibacterial agents against both Gram-positive and Gram-negative bacteria. From this study it is concluded that folic acid can be conjugated with other nanoparticles through electrostatic interaction for anticancer drug delivery.

References:

[1] X. Dai, Z. Fan, Y. Lu and P. C. Ray, *ACS Appl. Mater. Interfaces*, 2013, **5**, 11348-11354.

[2] S. M. Lee, H. J. Kim, Y. J. Ha, Y. N. Park, S. K. Lee, Y. B. Park and K. H. Yoo, *ACS Nano*, 2013, **7(1)**, 50-57.

[3] F. Jia, X. Liu, L. Li, S. Mallapragada, B. Narasimhan and Q. Wang, *Journal of Controlled Release*, 2013, **172**, 1020-1034.

[4] D. M. Tobaldi, C. Piccirillo, R. C. Pullar, A. F. Gualtieri, M. P. Seabra, P. M. L. Castro and J. A. Labrincha, *J. Phys. Chem. C*, 2014, **118**, 4751-4766.

[5] T. Angelova, N. Rangelova, R. Yuryev, N. Georgieva and R. Mulle, *Materials Science and Engineering C*, 2012, **32**, 1241–1246.

[6] S. P. Chakraborty, S. K. Mahapatra, S. Chattopadhyay, P. Pramanik and ***S***. Roy, *Asian Pacific Journal of Tropical Biomedicine*, 2011, **1(2)**, 102-109.

[7] J. Vidic, S. Stankic, F. Haque, D. Ciric, R. L. Goffic, A. Vidy, J. Jupille and B. Delmas, J. *Nanopart. Res.*, 2013 **15,** 1595-1605.

[8] C. Baker Austin, M. S. Wright, R. Stepanauskas and J. V. McArthur, *Trends Microbiol.***,** 2006, **14**, 176-182.

[9] A. J. Huh and Y. Kwon, *J. Control. Release*, 2011, **156**, 128-145.

[10] S. M. Dizaj, F. Lotfipour, Mo. B. Jalali, M. H. Zarrintana and K. Adibkia, *Materials Science and Engineering C*, 2014, **44,** 278–284.

[11] Y. H. Kim, C. W. Kim, H. G. Cha, D. K. Lee, B. K. Jo, G. W. Ahn, E. S. Hong, J. C. Kim and Y. S. Kang, *J. Phys. Chem. C*, 2009, **113**, 5105-5110.

[12] S. K. Gogoi, P. Gopinath, A. Paul, A. Ramesh, S. S. Ghosh and A. Chattopadhyay**,** *Langmuir***,** 2006**, 22(22),** 9322-9328.

[13] A. T. Le, L. T. Tama, P. D. Tama, P.T Huy, T. Q. Huy, N. V. Hieuc, A. A. Kudrinskiy and Y. A Krutyakov, *Materials Science and Engineering C*, 2010, **30**, 910–916.

[14] M. Wang, H. Hu, Y. Sun, L. Qiu, J. Zhang, G. Guan, X. Zhao, M. Qiao, L. Cheng, L. Cheng and D. Chen, *Biomaterials*, 2013, **34**, 10120-10132.

[15] D. Chen, P. Song, F. Jiang, X. Meng, W. Sui, C. Shu and L. J. Wan, *J. Phys. Chem. B*, 2013, **117**, 1261-1268.

[16] E. Roger, S. Kalscheuer, A. Kirtane, B. R. Guru, A. E. Grill, J. Whittum-Hudson, and J. Panyam, *Mol. Pharmaceutics*, 2012, **9**, 2103-2110.

[17] J. J. Lin, J. S. Chen , S. J. Huang , J. H. Ko, Y. M. Wang, T. L. Chen and L. F. Wang, *Biomaterials*, 2009, **30**, 5114-5124.

[18] S. K. Sahu, S. Maiti, A. Pramanik, S. K. Ghosh and P. Pramanik, *Carbohydrate Polymers*, 2012, **87**, 2593-2604.

[19] S. K. Sahu, S. Maiti, T. K. Maiti, S. K.Ghosh and P. Pramanik, *Macromolecular Bioscience*, 2011, **11(2)**, 285-295.

[20] S. J. Yang, F. H. Lin, H. M. Tsai, C. F. Lin, H. C. Chin, J. M. Wong and M. J. Shieh, *Biomaterials*, 2011, **32**, 2174-2182.

[21] A. Sulistio, J. Lowenthal, A. Blencowe, M. N. Bongiovanni, L. Ong, S. L. Gras, X. Zhang and G. G. Qiao, *Biomacromolecules*, 2011, **12**, 3469-3477.

[22] S. P. Chakraborty, S. K. Sahu, S. Kar Mahapatra, S. Santra, M. Bal, S. Roy and P. Pramanik, *Nanotechnology*, 2010, **21,** 105103-105112.

[23] J. T. Wu and L. C. Hsu Steve, *J.NanopartRes.*, 2011, **13**, 3877-3883.

[24] S. Sahu, B.Behera, T. K. Maiti and S. Mohapatra, *ChemComm.*, 2012, **48,** 8835-8837.

[25] M. J. Frisch, etal.Gaussian 03, Gaussian Inc., Pittsburgh, PA., 2003

[26] A. Frisch, I. I. R. Dennington, T. Keith, J. Millam, A. B. Nielsen, A. J. Holder, J. Hiscocks, Reference, Version 5.0, Gaussian Inc., Pittsburgh, 2007

[27] J. X. Wang, L. X. Wen, Z. H. Wang and J. F. Chen, *Mater. Chem. Phys.*, 2006, **96**, 90-97.

[28] H. M. Ericsson and J. C. Sherris, *ActaPathol. Microbiol. ScandB*, 1971, **217**, 1-10.

[29] A. Z. Melaiye, K. Sun, A.Milsted, D. Ely, D. H.Reneker, C. A.Tessier and W. J.Youngs, *J. Am. ChemSoc.*, 2005, **127**, 2285-2291.

[30] J. Y. Kim, K. Sungeun, J. Kim, L. Jongchan and J. Yoon, *Korean Soc. Environ. Eng.*, 2005, **27**, 771-776.

[31] G. Jin, H. Qin, H. Cao, S. Qian, ***Y***. Zhao, X. Peng, X. Zhang, X. Liu and P. K.Chu, *Biomaterials*, 2014, **35(27)**, 7699-7713.

[32] P. Pallavicini, A. Taglietti, G. Dacarro, Y. A. Diaz-Fernandez, M. Galli, P. Grisoli, M. Patrini, G. S. De Magistris and R. Zanoni, *Journal of Colloid and Interface Science*, 2010, **350**, 110-116.

[33] H. L. Sua, C. C. Choub, D. J. Hunga, S. H. Lina, I. C. Paoa, J. H. Linc, F. L. Huang, R. X. Dong and J. J. Linb, *Biomaterials*, 2009, **30**, 5979-5987.

[34] J. Shi, X. Sun, Y. Lin, X. Zou, Z. Li, Y. Liao, M. Du and H. Zhang, *Biomaterials*, 2014, 35, 6657-6666.

[35] P. Kolandaivel, G. Praveen and P. Selvarengan, *J. Chem. Sci.*, 2005, **117**, 591-598.

[36] F. J. Luque, J. M. Lopez and M. Orazco, *Theor. Chem. Acc.*, 2000, **103**, 343-345.

[37] N. Okulik and A.H. Jubert, *Int. Elect. J. Mol. Des.*, 2005, **4**, 17-30.

[38] L. Zhang, T. Ren, L. Zhou, J. Tian and X. Li, *Computational and Theoretical Chemistry*, 2013, **1019**, 1-10.

[39] W. Sun and R. D. Felice, *J. Phys. Chem. C*, 2012, **116**, 24954-24961.

[40] K. Kawahara, K. Tsuruda, M. Morishita and M. Uchida, *Dental Mat.*, 2000, **16**, 452-455.

Figure Captions

Figure 1(a) X-ray diffraction patterns of Ag@TEA and Ag@TEA@FA nanoparticles **(b)** FTIR spectra of Ag@TEA and Ag@TEA@FA nanoparticles. (Inset picture (i) Ag@TEA nanoparticles (ii) Ag@TEA@FA nanoparticles)

Figure 2(a) TEM image of folic acid conjugated Ag nanoparticles**. (b)** FE-SEM image of Ag@FA@TEA nanoparticles **(c)** the corresponding diameter distribution of nanoparticles from TEM image. **(d)** EDX spectrum

Figure 3 Fully optimized molecular geometry of folic acid (FA) obtained at HF/6-311g (d,p) level.

Figure 4 (a) Molecular Electrostatic Potential (MEP) of Folic Acid **(b)** MEP of TEA **(c)** MEP of Ag@TEA Cluster and **(d)** MEP of Di-TEA@Ag Cluster.

Figure 5 Conformers of TEA@Ag@FA and Di-TEA@Ag@FA Clusters. **(a)** Molecular Cluster 1, **(b)** Molecular Cluster 2, **(c)** Molecular Cluster 3, **(d)** Molecular Cluster 4, **(e)** Di-Molecular Cluster 1, **(f)** Di-Molecular Cluster 2, **(g)** Di-Molecular Cluster 3.

Figure 6 Determination of the minimum bactericidal concentration of **(a)** Ag@TEA@FA against *S. aureus*, **(b)** Ag@TEA@FA against E. coli, (a = 1 μg ml^{-1}, b = 5 μg ml^{-1}, c = 10 μg ml^{-1}, d = 25 μg ml^{-1}, e = 50 μg ml^{-1}, f 100 μg ml^{-1}). The diameter of inhibition zone surrounding (i) Ag@TEA and (ii) Ag@TEA@FA NPs impregnated disks **(c)** *S. aureus* **(d)** *E. coli*.

Figure 7 FESEM images of *E. coli*: (a) control; (b) *E. coli* treated with Ag@TEA@FA nanopartilces for 12 h; (. Black arrows: Damaged portions) (c) Growth curves of *S. aureus* (a: only bacteria; c: bacteria + Ag@TEA; e: bacteria + Ag@TEA@FA) and *E. coli* (b: only bacteria; d: bacteria + Ag@TEA; f: bacteria + Ag@TEA@FA) cells exposed to minimum inhibitory concentrations (μg/ml) of Ag@TEA and Ag@TEA@FA at normal condition.

Figure 8 Fluorescent Microscopic image (50 × magnification) of particle uptake assay.

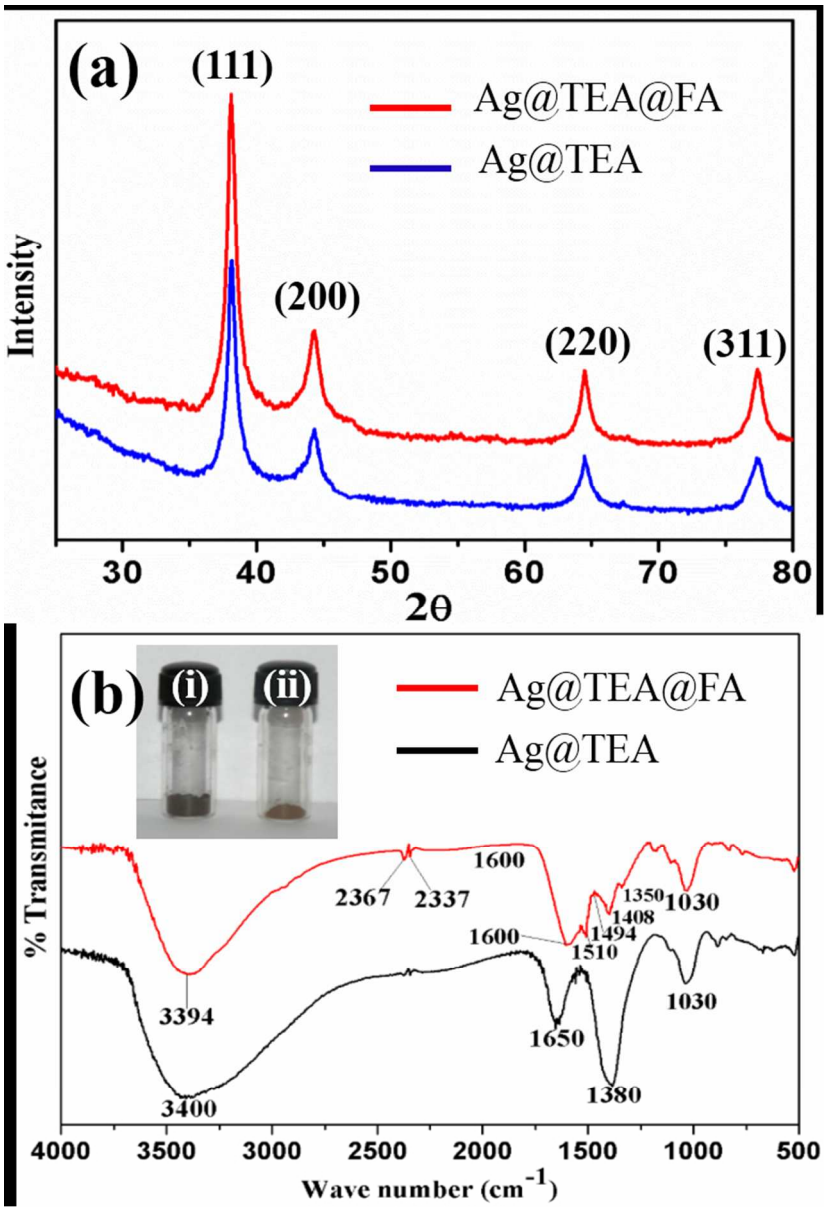

Figure 1(a) X-ray diffraction patterns of Ag@TEA and Ag@TEA@FA nanoparticles (b) FTIR spectra of Ag@TEA and Ag@TEA@FA nanoparticles. (Inset picture (i) Ag@TEA nanoparticles (ii) Ag@TEA@FA nanoparticles)
129x189mm (150 x 150 DPI)

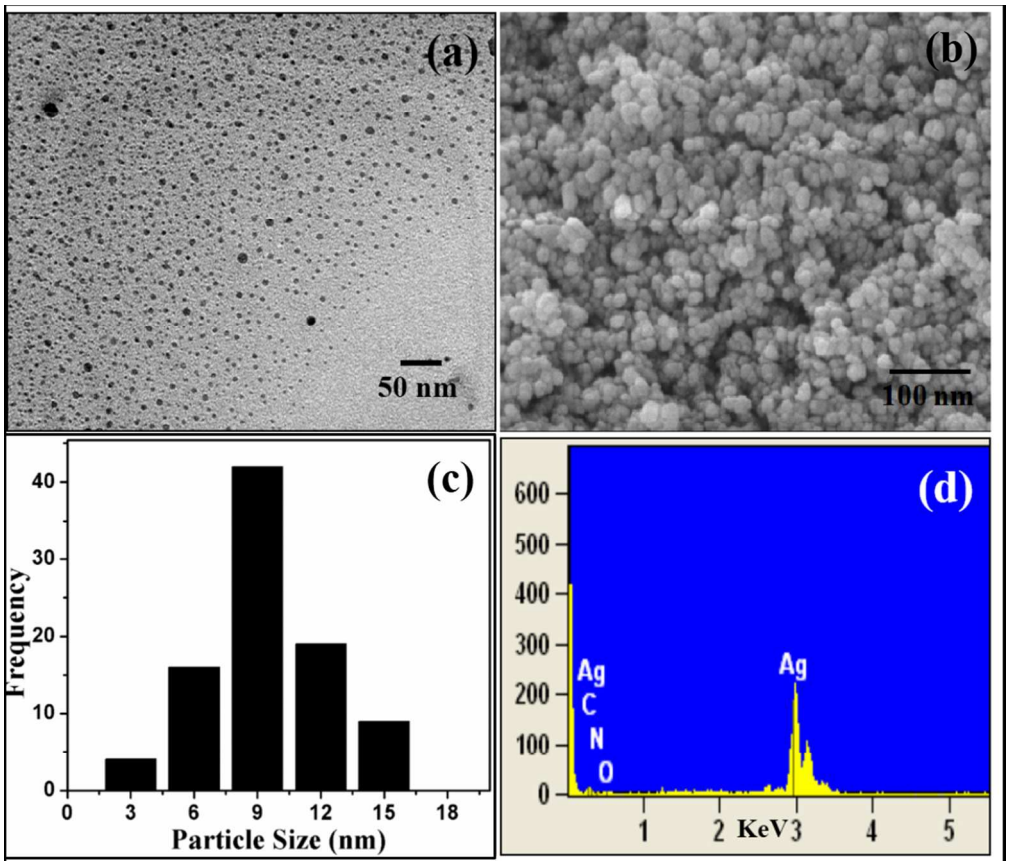

Figure 2(a) TEM image of folic acid conjugated Ag nanoparticles. (b) FE-SEM image of Ag@FA@TEA nanoparticles (c) the corresponding diameter distribution of nanoparticles from TEM image. (d) EDX spectrum
193x165mm (150 x 150 DPI)

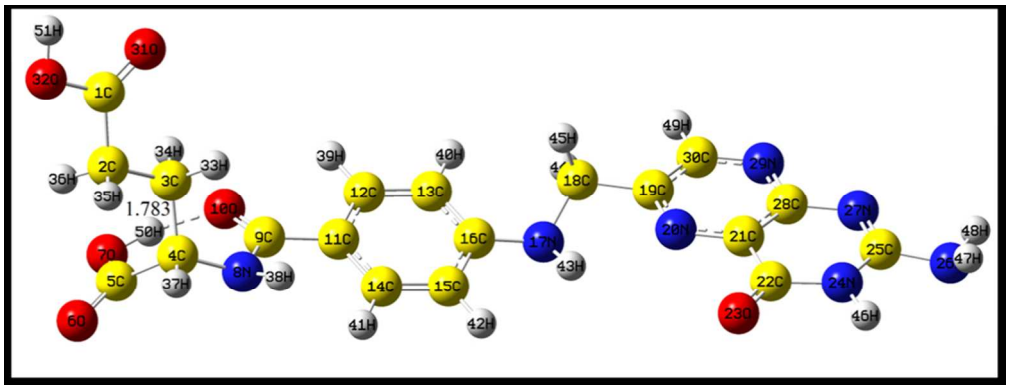

Figure 3 Fully optimized molecular geometry of folic acid (FA) obtained at HF/6-311g (d,p) level.
198x128mm (145 x 85 DPI)

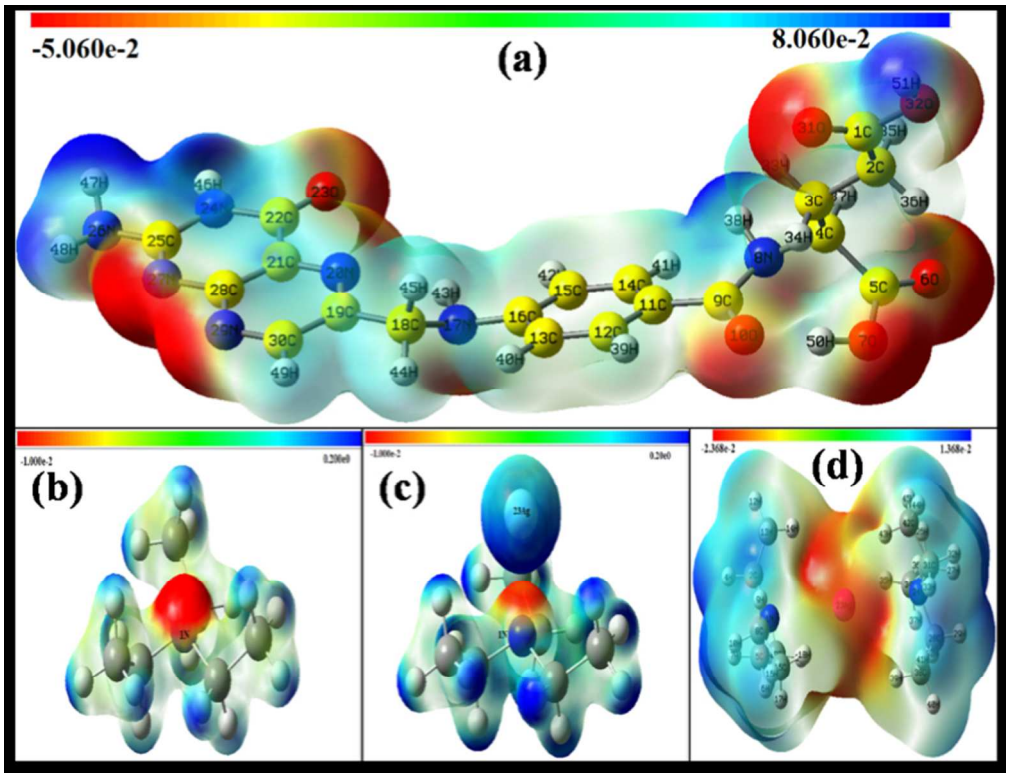

Figure 4 (a) Molecular Electrostatic Potential (MEP) of Folic Acid (b) MEP of TEA (c) MEP of Ag@TEA Cluster and (d) MEP of Di-TEA@Ag Cluster.
235x171mm (93 x 98 DPI)

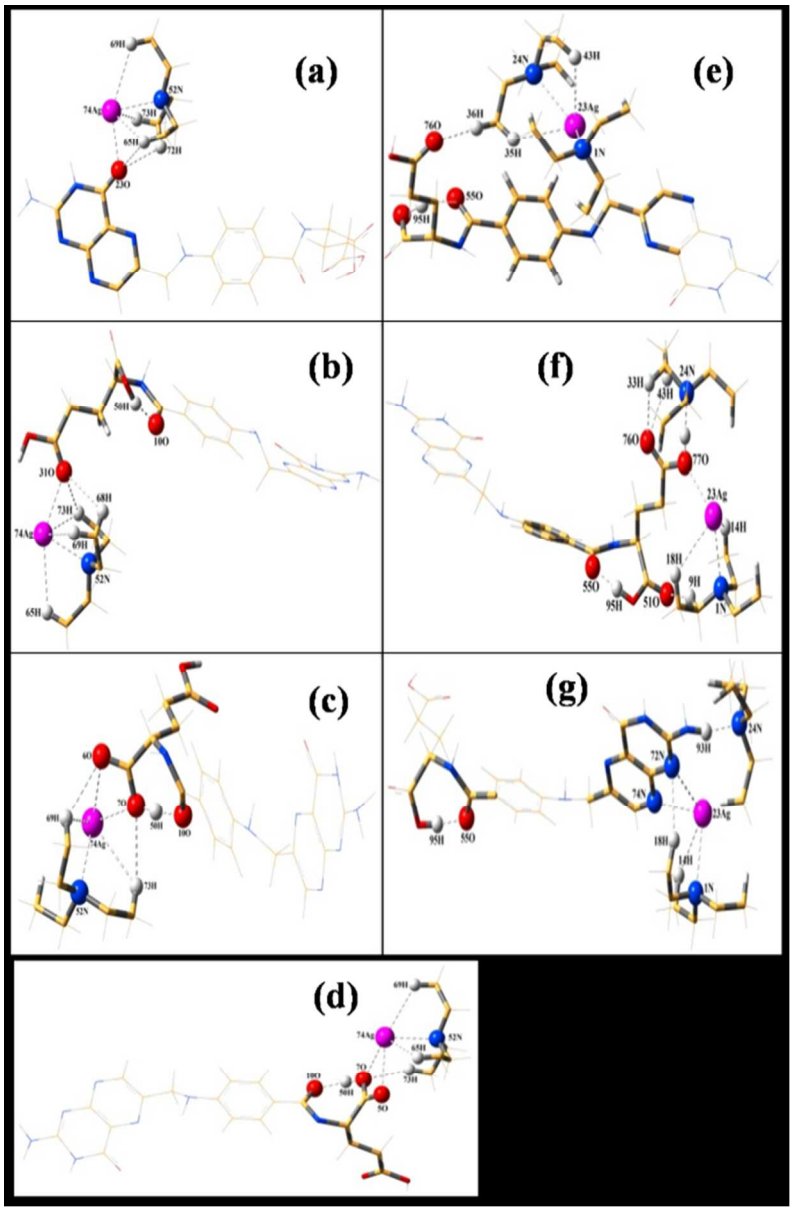

Figure 5 Conformers of TEA@Ag@FA and Di-TEA@Ag@FA Clusters. (a) Molecular Cluster 1, (b) Molecular Cluster 2, (c) Molecular Cluster 3, (d) Molecular Cluster 4, (e) Di-Molecular Cluster 1, (f) Di-Molecular Cluster 2, (g) Di-Molecular Cluster 3.
115x175mm (150 x 150 DPI)

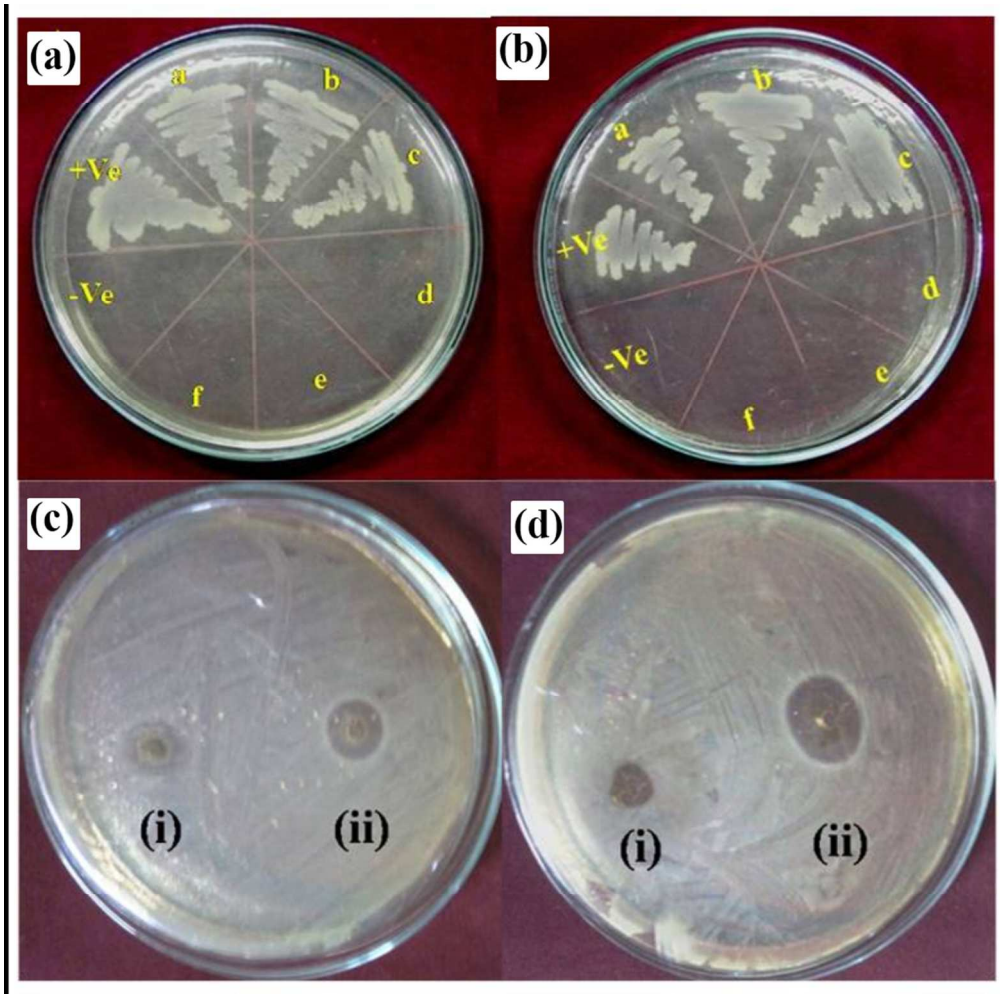

Figure 6 Determination of the minimum bactericidal concentration of (a) Ag@TEA@FA against S. aureus, (b) Ag@TEA@FA against E. coli, (a = 1 μg ml−1, b = 5 μg ml−1, c = 10 μg ml−1, d = 25 μg ml−1, e = 50 μg ml−1, f 100 μg ml−1). The diameter of inhibition zone surrounding (i) Ag@TEA and (ii) Ag@TEA@FA NPs impregnated disks (c) S. aureus (d) E. coli.
172x170mm (150 x 150 DPI)

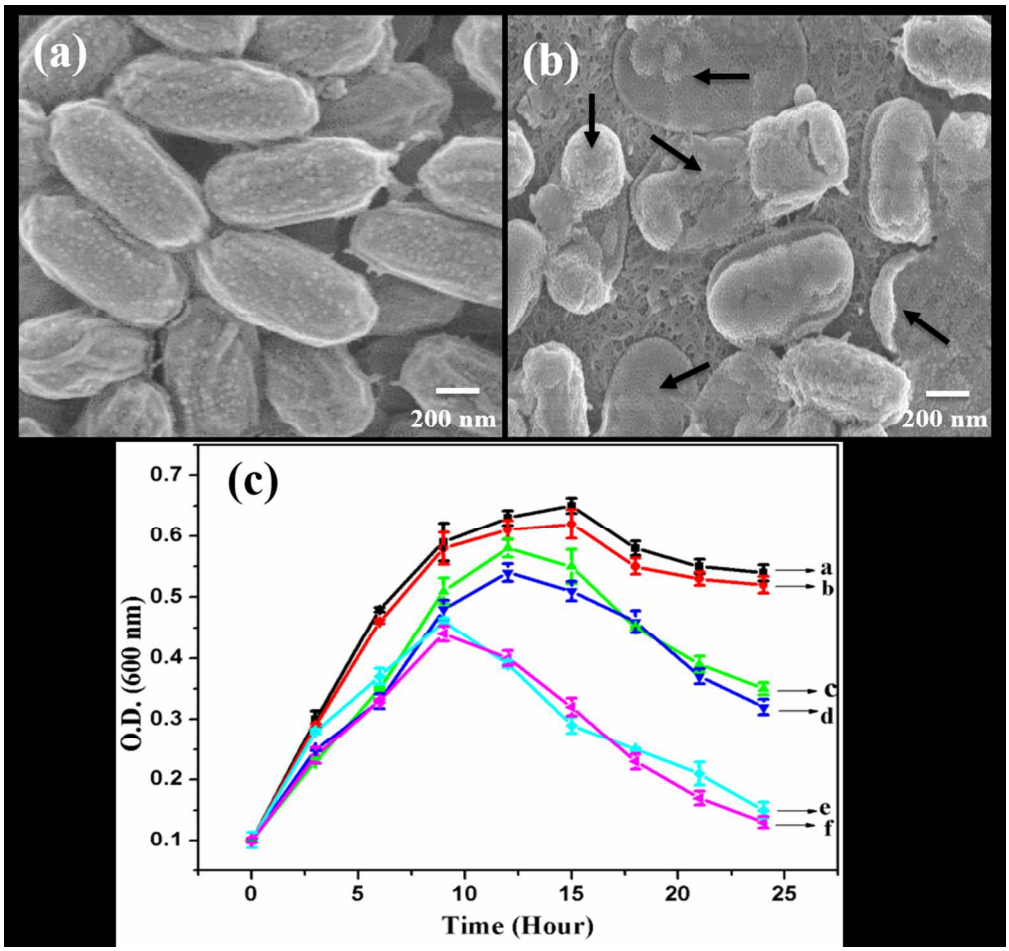

Figure 7 FESEM images of E. coli: (a) control; (b) E. coli treated with Ag@TEA@FA nanopartilces for 12 h; (. Black arrows: Damaged portions) (c) Growth curves of S. aureus (a: only bacteria; c: bacteria + Ag@TEA; e: bacteria + Ag@TEA@FA) and E. coli (b: only bacteria; d: bacteria + Ag@TEA; f: bacteria + Ag@TEA@FA) cells exposed to minimum inhibitory concentrations (μg/ml) of Ag@TEA and Ag@TEA@FA at normal condition.
179x169mm (150 x 150 DPI)

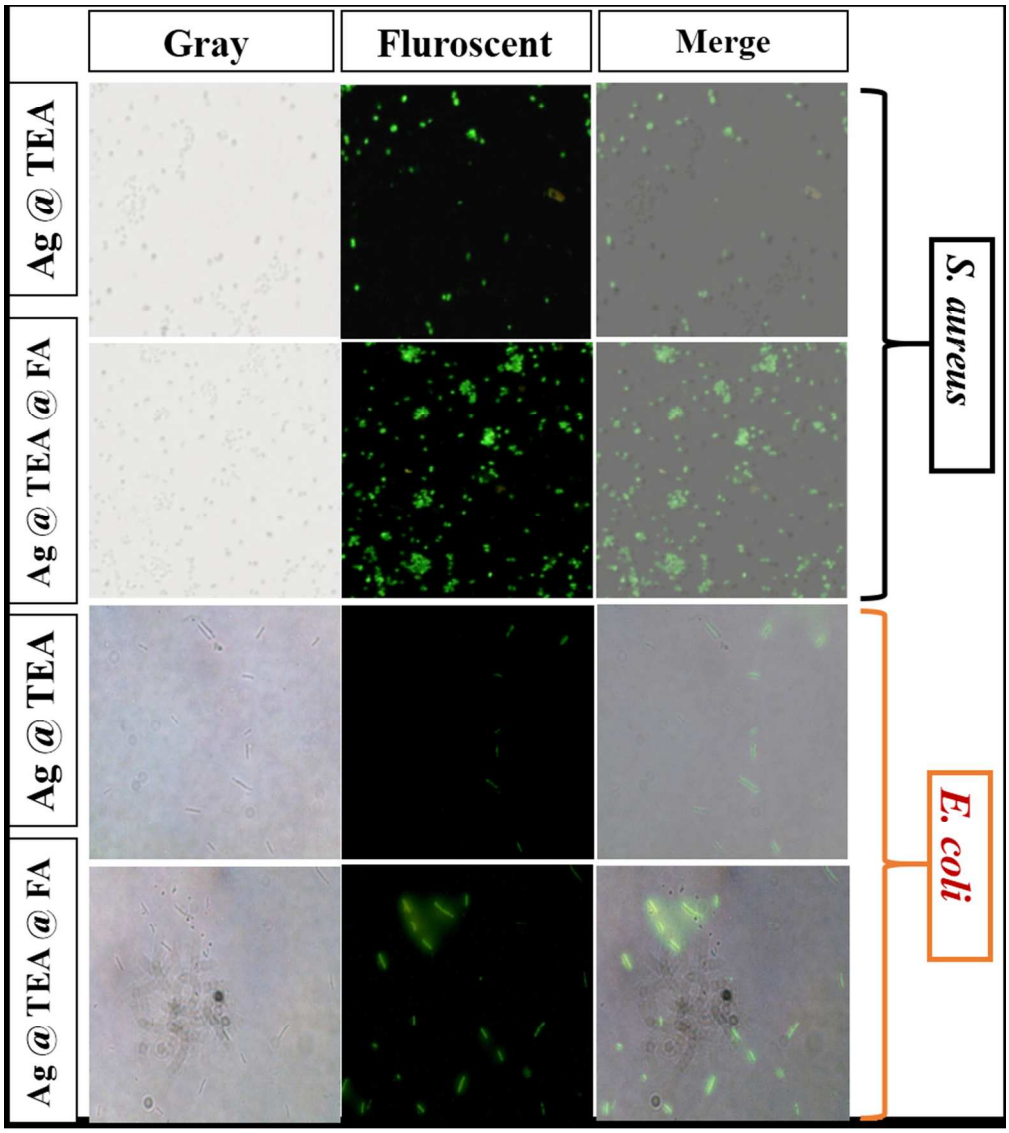

Figure 8 Fluorescent Microscopic image (50 × magnification) of particle uptake assay.
164x184mm (150 x 150 DPI)